Available online at www.sciencedirect.com
SCIENCE DIRECT®
Journal of Constructional Steel Research 62 (2006) 329–342
JOURNAL OF CONSTRUCTIONAL STEEL RESEARCH
www.elsevier.com/locate/jcsr

Shear strength of horizontally curved steel I-girders — finite element analysis studies

Se-Kwon Jung*, Donald W. White

Structural Engineering, Mechanics and Materials, Georgia Institute of Technology, Atlanta, GA 30332-0355, United States

Received 3 March 2005; accepted 16 August 2005

Abstract

This paper presents the results of finite element analysis (FEA) studies of four curved steel I-girder shear components tested experimentally in previous research, as well as parametric extensions of these tests. These studies focus on the influence of horizontal curvature on the maximum strength of transversely stiffened members with web slenderness D/t_w approximately equal to the largest value permitted in AASHTO [AASHTO LRFD bridge design specifications. 3rd ed. In: 2005 Interim Provisions, Washington (DC): American Association of State and Highway Transportation Officials; 2004], and with panel aspect ratios of $d_o/D = 1.5$ and 3.0. These ratios are larger than previously considered in experimental tests of curved I-girders with similar or larger slenderness. The girders studied have subtended angles between their bracing locations of $L_b/R = 0.05$ and 0.10, and web panel d_o/R values ranging from 0.03 to 0.10. The FEA models incorporate the measured material stress–strain relationships and section dimensions from the physical tests, detailed modeling of the test boundary conditions, residual stresses due to flame cutting and welding, and initial geometric imperfections in the form of buckling mode shapes. The load transfer mechanisms of the test girders are investigated via elastic buckling and full nonlinear analyses. The parametric studies are performed to investigate the effects of residual stresses and geometric imperfections, the behavior of equivalent straight girders, and the influence of reduced flange size on the peak shear capacity and moment–shear interaction.

Keywords: Steel bridges; Curved bridges; Shear strength; Tension field action; Postbuckling resistance

1. Introduction

In Zureick et al. [28], the results of experimental shear strength tests of four full-scale curved I-girder components are presented. Fig. 1 shows a schematic of the test set-up, and Fig. 2 shows a photograph taken from the right side of location 1R (defined in Fig. 1). These component tests were designed to investigate the influence of horizontal curvature on the postbuckling shear response of I-girders with:

- web slenderness D/t_w approximately equal to the largest value permitted for transversely stiffened members in [2], and
- panel aspect ratios of $d_o/D = 1.5$ and 3.0, which are larger than previously considered in experimental tests of curved I-girders with similar or larger D/t_w values.

This paper presents the results from finite element analyses (FEA) of these physical tests as well as parametric variations based on these girders. Both the elastic shear buckling and the full nonlinear maximum shear strength responses are considered. The parametric studies investigate (1) the effect of residual stresses on the curved I-girder shear strength response, (2) the sensitivity of the shear strengths to geometric imperfections, (3) differences and similarities between the behavior of the curved I-girders and equivalent straight I-girders, and (4) the influence of flange size on the shear strength behavior of and moment–shear interaction within curved I-girders.

The AASHTO [2] shear strength provisions are essentially the same as those in prior AASHTO straight bridge specifications, but permit the use of the same postbuckling shear resistance for both straight and curved transversely stiffened I-girders with $D/t_w \leq 150$ and $d_o/D \leq 3.0$. Also, the AASHTO [2] provisions do not require the consideration of any interaction between the flexural and shear resistances.

* Corresponding author. Tel.: +1 404 894 9354; fax: +1 404 894 2278.
E-mail addresses: gtg426c@prism.gatech.edu (S.-K. Jung), dwhite@ce.gatech.edu (D.W. White).

0143-974X/$ - see front matter © 2005 Elsevier Ltd. All rights reserved.
doi:10.1016/j.jcsr.2005.08.003

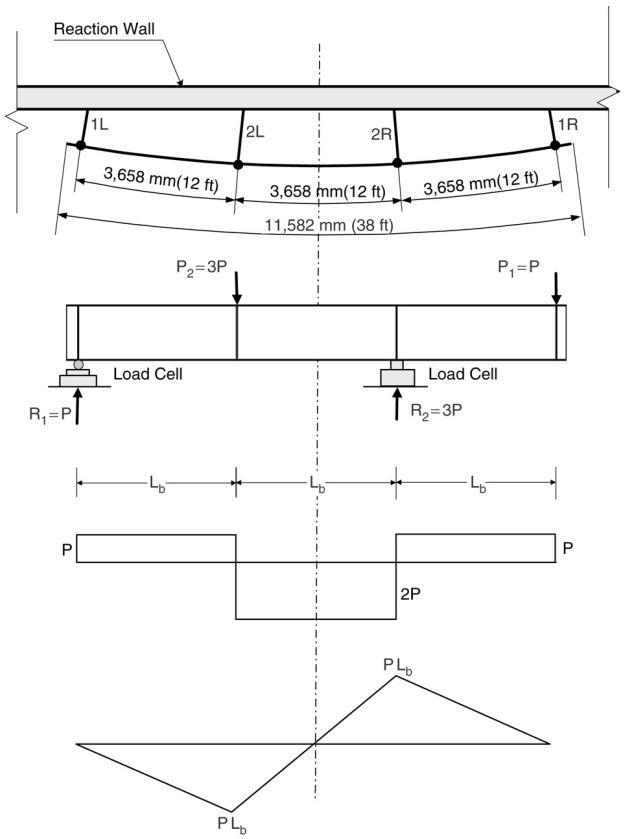

Fig. 1. Test set-up and shear and approximate moment diagrams, from [28].

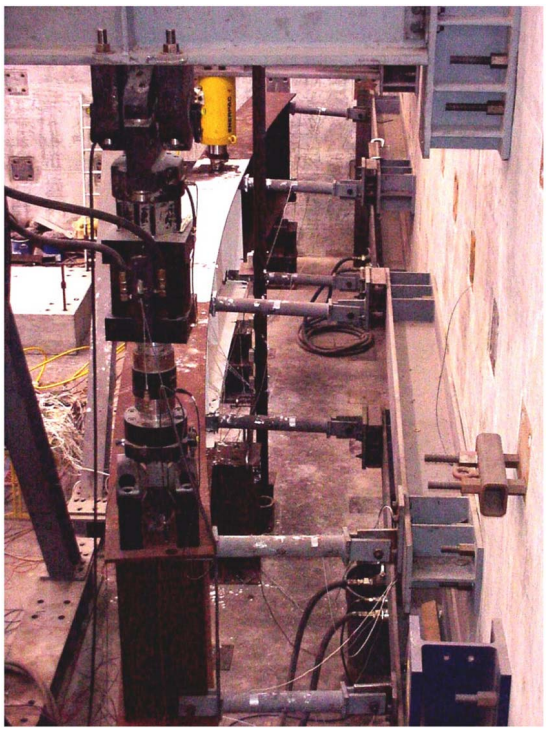

Fig. 2. Longitudinal view of test set-up from end 1R, from [28].

Overall characteristics of the four physical test girders from [28] and outlines of the specific objectives of each of the experimental tests are described in the following section. This is followed by a summary of the measured geometries utilized in the FEA models, the overall modeling approach, the FEA mesh discretization, the idealization of the load and displacement boundary conditions, the physical stress–strain response and its characterization within the analysis, the calculated representative nominal residual stresses, and the initial geometric imperfections defined within the analysis models. Subsequently, the results of analyses of the four physical test girders are presented followed by the results of the various parametric studies.

2. Girder geometry

Zureick et al. [28] conducted four full-scale curved steel I-girder component shear tests. Two of the girders, labeled S1 and S1-S, had a nominal radius $R = 63,630$ mm (208.75 ft) and a transverse stiffener spacing such that the ratio d_o/D was 3 for S1 and 1.5 for S1-S (producing $d_o/R = 0.0575$ and 0.03). The other two components, labeled S2 and S2-S, were identical to S1 and S1-S except that their radii were 36,580 mm (120 ft), resulting in $d_o/R = 0.10$ and 0.050. Figs. 3–5 illustrate the overall geometry of the test girders and define labels used in the subsequent sections of this paper.

Each of the test girders had a total arc length of 11,580 mm (38 ft) and a doubly symmetric cross section with nominally 544.5 × 22.2 mm (21–7/16 × 7/8 in.) flange plates that were cut curved and 1219 × 8 mm (48 × 5/16 in.) web plates that were heat curved. The resulting web slenderness D/t_w was 154, the flange slenderness $b_f/2t_f$ was 12.25, and the ratio of the web-to-flange area A_w/A_f was 0.8 based on these nominal dimensions. The value of $D/t_w = 154$ is approximately equal to the maximum value of $D/t_w = 150$ permitted for transversely stiffened I-girders in [2]. All the girders had four 229 × 25.4 mm (9 × 1 in.) bearing stiffeners placed in pairs at 305 mm (1 ft) from their ends and at 3660 mm (12 ft) intervals along their length under each load point. All the above plates were connected to the web and flanges by 6.35 mm (1/4 in.) fillet welds. The girders were braced radially at each of the bearing stiffener locations such that the unsupported lengths along the girder arc were $L_b = 3658$ mm (12 ft) and the ratio L_b/b_f was 6.7 in all the girders. Two 101.6 mm (4 in.) diameter steel tubes with nominal area 1802 mm^2 were connected through spherical bearings to the stiffeners at locations near the top and bottom flanges, and to a large reaction wall at their opposite ends (see Figs. 1 and 2). At the beginning of the tests, the attachment of the bracing to the girders was approximately 50.8 mm (2 in.) higher than the attachment to the reaction wall. The length between the spherical bearings at the ends of the bracing members was 1028.7 mm (40.5 in.) at locations 1L and 1R and 1244.6 mm (49 in.) at locations 2L and 2R.

Table 1 presents a matrix of nondimensional parameters associated with the four tests, including the parameters c and Z, which are curvature parameters defined as

$$c = \frac{d_o^2}{8Rt_w} \tag{1}$$

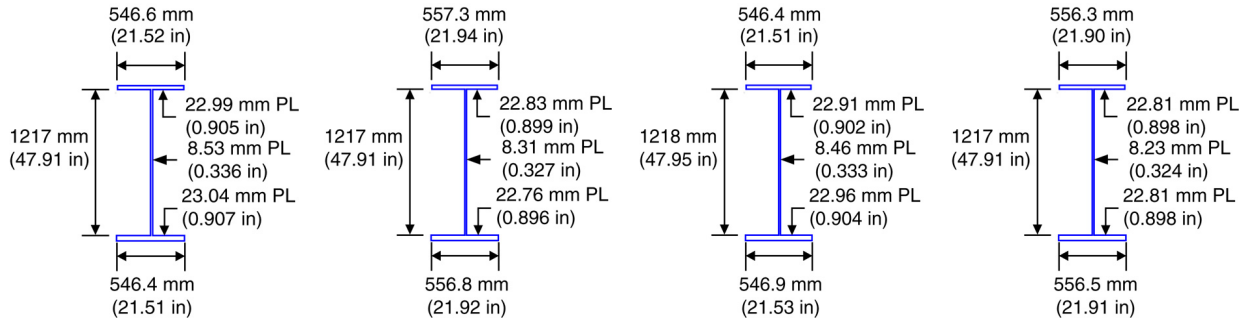

(a) S1 cross-section. (b) S2 cross-section. (c) S1-S cross-section. (d) S2-S cross-section.

Fig. 3. Measured cross-section dimensions, from [28].

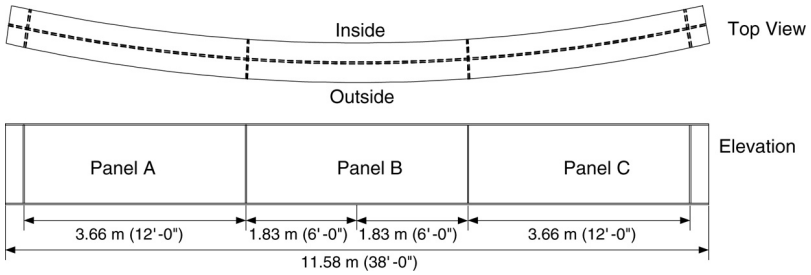

Fig. 4. Geometry and longitudinal dimensions of test girders S1 and S2, from [28].

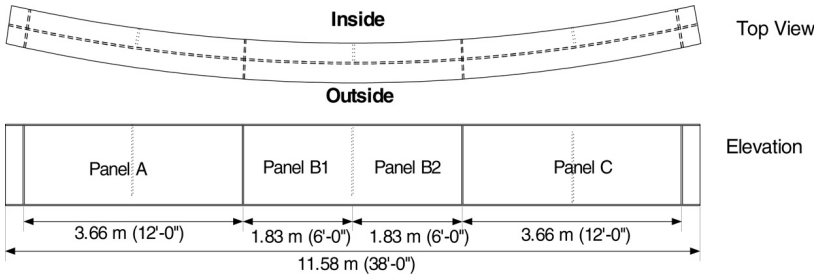

Fig. 5. Geometry and longitudinal dimensions of test girders S1-S and S2-S, from [28].

Table 1
Summary of test girder nondimensional parameters

Girder	L_b/R	d_o/D	d_o/R	c	Z
S1	0.0575	3	0.0575	3.31	25.3
S1-S	0.0575	1.5	0.03	0.83	6.3
S2	0.10	3	0.1000	5.76	44.0
S2-S	0.10	1.5	0.0500	1.44	11.0

and

$$Z = d_o^2\sqrt{1-\nu^2}/Rt_w = 8c\sqrt{1-\nu^2}. \quad (2)$$

The parameter c is a small-angle approximation of the maximum eccentricity of the curved web from a chord between the ends of the panel, divided by the web thickness. The term Z is used in the [1] stiffener design equations to account for the influence of horizontal curvature.

The value of c for all but one of these designs is significantly greater than one. This is due to the large panel aspect ratios d_o/D and web slenderness D/t_w relative to prior practice as reflected in [1] and in [20].

3. Objectives of physical tests

The objectives of each of these tests were as follows:

3.1. Girder S1

This test was targeted to examine the shear strength of a curved web panel having an aspect ratio of $d_o/D = 3$, a ratio of the web panel length to the radius of curvature of $d_o/R = 0.0575$, and a subtended angle between the cross frame locations of $L_b/R = 0.0575$. The angle $L_b/R = 0.0575$ is slightly greater than one-half of the maximum value of 0.10 permitted in the unified provisions for design of straight and curved I-girders in [2]. The web of this girder contained only the four bearing stiffeners described above without any intermediate transverse stiffeners.

3.2. Girder S1-S

This girder was identical in length and curvature to S1 but had an additional 165 × 16 mm (6–1/2 × 5/8 in.) intermediate

Table 2
Average engineering stress–strain data from tension coupon tests

Girders	Coupon location	E (GPa (ksi))	Static F_y (MPa (ksi))	E_{st} (GPa (ksi))	ε_{st} (%)	F_u (MPa (ksi))	ε_u (%)
S1 & S1-S R = 63,630 mm (208.75 ft)	Web	208 (30,189)	410 (59.5)	3.44 (499)	1.95	567 (82.3)	14.6
	Flanges	196 (28,447)	377 (54.7)	3.59 (521)	1.59	542 (78.7)	15.6
S2 & S2-S R = 36,580 mm (120 ft)	Web	202 (29,318)	411 (59.6)	3.36 (488)	1.87	564 (81.9)	15.6
	Flanges	205 (29,753)	397 (57.6)	3.61 (524)	1.90	562 (81.6)	15.4

transverse stiffener located at the center of each panel between the bearing stiffeners. The intermediate transverse stiffeners were cut back 25.4 mm (1 in.) from the tension flange in panels A and C (see Fig. 5) and from the bottom flange in panel B, and were placed on the side of the web closest to the center of curvature only. The resulting web panel aspect ratio was 1.5, and the value of d_o/R was 0.03. Although the above transverse stiffeners had reasonable proportions relative to the girder geometry, their moment of inertia about the edge in contact with the web plate is 52 times that required by [2]. The transverse stiffener size was selected conservatively to ensure that the shear strength would not be limited by a failure of the stiffener.

3.3. Girder S2

This component was similar to S1 in that it only had bearing stiffeners at 3658 mm (12 ft) intervals along its length and a resulting panel aspect ratio of $d_o/D = 3$. However, it differed from S1 in that it had a radius of 36,580 mm (120 ft), thus representing a case in which $L_b/R = 0.10$, the maximum subtended angle between the cross frame locations allowed by [2]. The corresponding d_o/R for this girder was 0.10. Since AASHTO [2] requires $L_b/R \leq 0.10$ within the final constructed configuration, and since connection plates are required at cross-frame locations, this girder represents the largest possible combination of d_o/R and L_b/R possible within these specifications.

3.4. Girder S2-S

This girder was identical to S1-S but had a radius of 36,580 mm (120 ft). Therefore, its normalized dimensional parameters were $d_o/D = 1.5$, $d_o/R = 0.050$, and $L_b/R = 0.10$.

Table 2 summarizes the mean values of the following key stress–strain parameters determined from tension tests: the modulus of elasticity E, the static yield F_y, the strain hardening modulus E_{st}, the strain at the onset of strain hardening e_{st}, the ultimate tensile strength F_u, and the ultimate strain e_u. Details of how these parameters were determined from the tension coupon tests and statistics of the material test data are provided in [28]. The average E for all the tension specimens is 203 GPa (29,440 ksi) with a coefficient of variation of 2.6% [28] and is selected for Young's modulus to represent all of the analysis studies in this research. Fig. 6 shows the true stress–true strain curve from typical tension tests of the flange plates for girders S2 and S2-S along with a multilinear representation of the stress–strain response used within the analysis models.

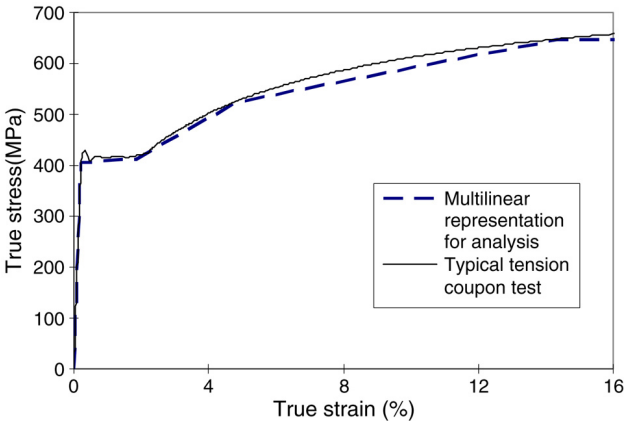

Fig. 6. Typical true stress–strain response.

4. Finite element discretization

Fig. 7 shows a typical FEA model used in this research. The models are constructed within the ABAQUS 6.3 analysis system [10] using the S4R element, a four-node quadrilateral displacement-based shell element with reduced integration. The shell elements use five integration points and a trapezoidal integration rule in the thickness direction. In the construction of the FEA models, ten elements are used through the width of the flanges, and twenty elements are used through the depth of the web in all the specimens. The elements at the ends of the bearing stiffeners are constrained to the corresponding top and bottom flange nodes, whereas the ends of the transverse stiffeners (one-sided) are stopped one element short of the flange they are cut short of but are constrained to the other flange. The T31 truss element is used to represent the tube braces shown in Fig. 2. It was found that the above level of mesh refinement results in adequate convergence of the predicted displacements and strains.

Fig. 7 also illustrates specified boundary conditions within the FEA models. The exterior vertical support at location 1L is modeled by restraining the displacements in the vertical direction along a line across the width of the bottom flange. That is, an ideal roller support is specified, and the girders are

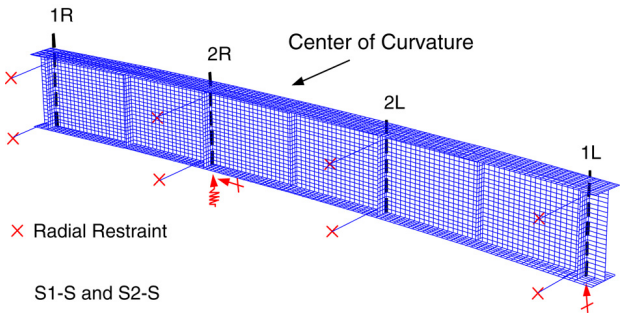

Fig. 7. Typical FEA model with specified boundary conditions.

free to move along the tangential direction at this location. The interior vertical support at location 2R is assumed to be rigid in compressive contact over the full area of the bearing plate, but uplift is allowed at any locations of the bottom flange that would tend to lift off of the bearing plate due to the deformations of the girder. Equivalent spring elements with a large elastic stiffness in compression and zero stiffness for net tension are used over the bearing plate area to represent this boundary condition. The tangential displacement is assumed to be restrained at the middle of the bottom flange at location 2R. That is, it is assumed that the bearing plate prevents displacements tangent to the arc of the girder at this location, thus preventing rigid body motion of the girder in the circumferential direction.

With regard to the force boundary conditions used in the analysis, concentrated loads with a total magnitude of 3P and P are applied at the interior brace location 2L and at the end brace location 1R, respectively. Each of these loads is subdivided into three concentrated loads, with three-quarters of the total load placed at the web–flange juncture and one-eighth applied on each side of this position. The FEA models also include the self-weight of the test girders and of the bracing members.

Furthermore, the FEA models include residual stresses due to flame cutting and welding of the flanges to the web in the fabrication process. The pattern and magnitude of these initial stresses are based on ECCS (1976), which provides a number of simple equations for estimating residual stresses. Residual stresses due to heat curving are not considered in the present research, but are addressed in [24]. Also, transverse normal residual stresses in the web due to welding of the stiffeners are not considered. The resulting residual stresses shown in Fig. 8 are used as representative values in this research.

Together with residual stresses, the inevitable presence of geometric imperfections generally influences the resistance of steel structures. Initial geometric imperfections change the structural stability behavior of elements such as flat web panels from a bifurcation problem to a load–deflection problem. For an imperfect web panel, the transverse (or radial) displacements increase gradually from the onset of the loading. Furthermore, due to stable postbuckling characteristics, the structure may sustain loads greater than the theoretical buckling load. In fact, the theoretical buckling load may be quite difficult to discern from experimental testing results, e.g., see [4].

In horizontally curved I-girders, the horizontal curvature itself acts as a geometric imperfection such that the analysis solution is generally a load–deflection problem. However, it

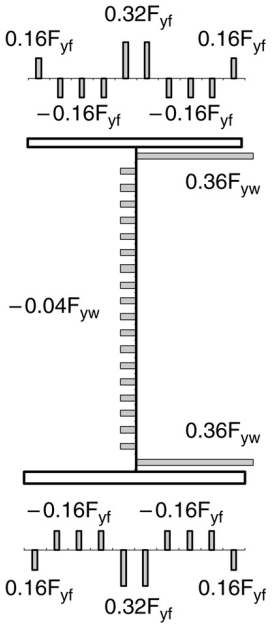

Fig. 8. Gauss point residual stresses used within the majority of the FEA studies in accordance with ECCS, 1976, based on flame cutting and consecutive placement of 7.93 mm (5/16 in.) web-to-flange fillet welds.

Table 3
Measured maximum web out-of-flatness, from [28]

Girder	Out-of-flatness δ_o (mm (in.))	$\frac{\delta_o}{t_w}$	$\frac{\delta_o}{(d/67)}$
S1	3 (0.118)	0.352	0.165
S1-S	3 (0.113)	0.339	0.158
S2	5 (0.197)	0.602	0.275
S2-S	8 (0.315)	0.972	0.440

is still possible for imperfections such as the web out-of-flatness (or initial radial displacements) relative to the perfect horizontally curved geometry to have some impact on the stability behavior and maximum strength. Table 3 shows the values for the measured maximum out-of-flatness of the web relative to a chord between the top and bottom of the web panels from [28]. These imperfections were estimated by placing a straight edge between the top and bottom of the web in a vertical position at various locations along the length and then measuring the gap between the straight edge and the web panel with a scale to the nearest millimeter. The largest imperfections located between the interior bearing stiffeners in each of the girders were all oriented toward the inside direction, i.e., toward the center of curvature. These imperfections were measured on the girders after they were placed on the supports at locations 1L and 2R and the bracing members were attached (see Figs. 1 and 2), but prior to the application of the applied concentrated loads at locations 2L and 1R. The ratio of these out-of-flatness values to the web thickness, and to the maximum value permitted by the AWS Structural Welding Code [3] in interior girders with one-sided stiffeners (equal to $d/67$ where d is the least panel dimension) is also shown in the table.

In this research, the nominally perfect geometry (based on the nominal horizontal curvature) is perturbed by representative imperfections in the shape of selected buckling modes.

Table 4
Predicted panel shear buckling loads

Girder	d_o/D	D/t_w	V_{cr} (FEA) (kN (kips))	AASHTO V_{cr}/V_{cr} (FEA)	Modified AASHTO V_{cr}/V_{cr} (FEA)
S1	3	143	837(188)	0.63	0.99
S2	3	146	801(180)	0.60	0.95
S1-S	1.5	144	948(213)	0.70	0.98
S2-S	1.5	148	912(205)	0.67	0.94

The buckling modes are dominated generally by radial web displacements, i.e., by web out-of-flatness relative to the perfect horizontally curved geometry. The first mode for S1-S and S2-S and the second mode for S1 and S2 are scaled by the magnitude of the web out-of-plumbness, which generates the maximum amplitude of imperfections toward the center of curvature. These choices for the geometric imperfections give the smallest or close to the smallest maximum strengths from numerous imperfection patterns considered for all four test girders [15]. Unless noted otherwise, the resulting imperfections are specified such that the maximum web out-of-flatness δ_o is equal to the value specified in Table 3. Flange sweep and tilt relative to the perfect horizontally curved geometry are assumed to have a minor impact on the girder responses.

5. Results and discussion

5.1. Elastic shear buckling analysis

I-girder design shear strengths are based in part on the theoretical elastic shear buckling load of the web. Table 4 compares the elastic shear buckling loads determined by the AASHTO [2] equations, and by a modification to these equations using the shear buckling coefficient equations developed by Lee et al. [16], to the buckling loads from FEA. The shear buckling coefficient equations are summarized in [27].

One can observe that the AASHTO predictions are much lower than the values obtained by the FEA. This is because the AASHTO elastic shear buckling load is based on the assumption that all four edges of a web panel are simply supported. The underestimation of the buckling strength by this simplified representation is as large as 40% (Girder S2) and depends to some extent upon the aspect ratio of the web panels (the predictions are slightly better for the girders with smaller d_o/D). With the use of the shear buckling coefficient formulae suggested by Lee et al., the predicted elastic shear buckling strength is within 90% of the FEA prediction for all the girders. These results, combined with those from other studies by White et al. [24], Bradford [5], and Lee et al. [16], indicate that significant conservatism associated with the prediction of the elastic shear buckling strength can be alleviated by adopting the shear buckling coefficients suggested by Lee et al.

5.2. Full nonlinear analysis of test girders

Table 5 shows that the physical test strengths were slightly smaller than the values obtained from the FEA for all of the girders (see the fourth column of the table). The strengths measured in the physical tests ranged from 89% to 97% of the maximum FEA strengths. Some of the potential reasons for these smaller test strengths are discussed subsequently. The greatest difference between the experimental and FEA results is for girder S1-S. Interestingly, the measured shear strengths based on $V_L = P_2 - R_1$ versus $V_R = R_2 - P_1$ (see Fig. 1) were within less than two percent of one another in all of the tests except for S1-S, where V_R/V_L was 1.067. The experimental shear values are based on the average of V_L and V_R. If the larger of these two values ($V_R = 1410$ kN) is used for girder S1-S, the ratio of the test to the FEA shear strength is 0.92. Therefore, depending on how one calculates the measured experimental shear capacity, the experimental shear strength is approximately 8%–11% smaller than the FEA shear strength for the girders with the larger radius of curvature (i.e., girders S1 and S1-S), and it is approximately 3%–5% smaller than the FEA shear strength for the girders with the smaller radius of curvature (i.e., girders S2 and S2-S).

The FEA solutions exhibit the expected trend in which the maximum shear strength is reduced by increasing the horizontal curvature (i.e., by decreasing the radius of curvature R). The strength is reduced by 130 kN (or 10%) by the increase in d_o/R (or L_b/R) from 0.0575 in S1 to 0.10 in S2, and it is reduced by 46 kN (or 3%) by the increase in d_o/R from 0.03 in S1-S to 0.050 in S2-S. The experimental strength of girder S2 is 40 kN (3%) smaller than that of S1. However, the experimental strength of S2-S is 40 kN (3%) larger than that of S1-S. The FEA strengths are taken as the reference values for evaluation of the shear strength equations in the following discussion.

The AASHTO [2] shear strength equations closely match the FEA strengths for girders S1-S and S2-S (see the fifth column of Table 5). However, these equations tend to significantly underpredict the FEA strengths for the girders with the wider stiffener spacing (i.e., girders S1 and S2). When these equations are modified by the shear buckling coefficient per Lee et al. [16], the FEA strengths for S1 and S2 are predicted well but the strengths from the FEA of S1-S and S2-S are slightly overpredicted. The shear strength equations proposed by Lee and Yoo [17–19] significantly overestimate the FEA strengths for girders S1 and S2 and produce conservative results that are slightly less accurate than the AASHTO [2] equations for S1-S and S2-S. The equations from [11–13], as modified by White and Barker [27], provide arguably the best overall match with the FEA shear strengths for all the girders (the predictions by the modified AASHTO equations are of similar accuracy but tend to err more toward the liberal side of the FEA strengths whereas the equations from Höglund err more toward the

Table 5
FEA, measured, and predicted shear strengths

Girder	FEA V_{max} (kN (kips))	Test V_{max} (kN (kips))	V_{max}(Test)/ V_{max}(FEA)	V_n (AASHTO)/V_{max} (FEA)	V_n (Modified AASHTO)/V_{max} (FEA)	V_n (Lee and Yoo)/V_{max} (FEA)	V_n (Höglund) /V_{max} (FEA)	V_n (Cardiff)/V_{max} (FEA)
S1	1317 (296)	1200 (270)	0.91	0.80	0.97	1.11	0.99	0.99
S2	1187 (267)	1160 (260)	0.97	0.85	1.02	1.19	1.05	1.04
S1-S	1531 (344)	1370 (307)	0.89	1.00	1.09	0.97	0.97	1.10
S2-S	1485 (334)	1410 (317)	0.95	0.99	1.07	0.98	0.97	1.10

conservative side). Lastly, the form of the Cardiff equations [7, 23,9,8] suggested by White and Barker [27] provides a good estimate of the FEA capacities for girders S1 and S2, but gives liberal predictions relative to the FEA results that are comparable to those of the Modified AASHTO equations for girders S1-S and S2-S.

5.2.1. Load–displacement (vertical and radial) responses

Figs. 9–12 compare the shear versus vertical deflections at location 2L determined by the full nonlinear analysis to the corresponding measured shear versus vertical deflections at the applied load positions 2L and 1R. Given the fact that the vertical deflections in the FEA at both locations 2L and 1R are essentially the same until the peak capacity is reached and only slightly different in the post-peak region, only the FEA deflection at location 2L is plotted in the figures. However, the measured deflections at both locations 2L and 1R are included, since these deflections differed significantly from one another. The differences between the vertical displacements within the physical tests are believed to be related to the control of the tests by maintaining the ratio of the interior to exterior applied load constantly close to three (see Fig. 1). Since the relative displacements of locations 2L and 1R were not controlled directly within the tests, these displacements tended to drift.

The overall shear–vertical displacement curves are very similar between the FEA solutions and the experimental tests for the girders with $d_o/D = 3$. On the other hand, at the end of the post-peak range of the response (i.e., at approximately 51 mm (2 in.) vertical displacement of the load points), the shear resistance is 22% and 9% smaller in the experiment than in the FEA solutions for the girders S1-S and S2-S, respectively. The FEA solutions suggest that the girders with the smaller stiffener spacing are able to sustain substantial inelastic shear deformations without any loss in the shear capacity. Conversely, the physical girders reached their maximum resistance and exhibited a mild decrease in their shear strengths with the onset of significant inelastic vertical displacements.

With the above exception, there is good correlation between the overall trends of the experimental test results and the FEA solutions with respect to the load–vertical and load–radial displacement responses, the wave patterns developed within the critical web panel(s), and the bending deformations developed within the flanges (associated with the frame action of these elements).

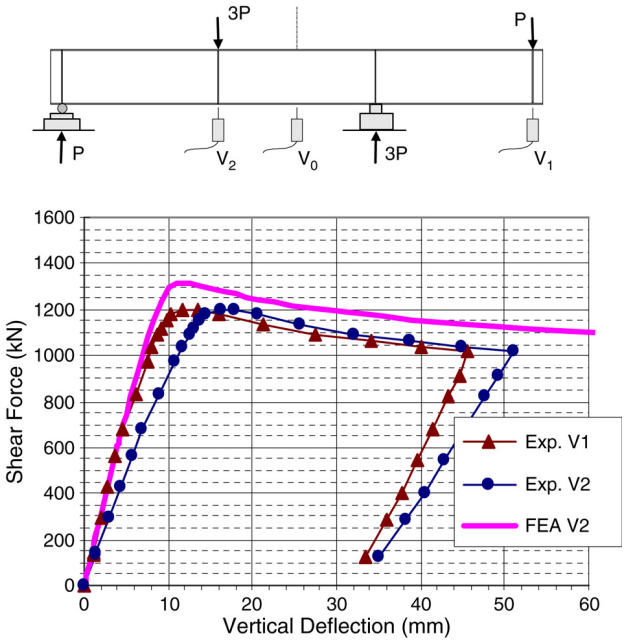

Fig. 9. Girder S1 — load–vertical deflection curves at the applied-load locations.

In the girders with $d_o/D = 1.5$, the vertical deflection of the bottom flange at the center of the test length reverses direction and actually moves upward depending on whether the final localized deformations occur within the left or the right-hand side web panel within this length. In the girders with $d_o/D = 3$, the bottom flange pushes up into the web within the post-peak range of the response in both the analyses and the experimental tests [15].

Figs. 13 through 16 compare the FEA load–maximum radial deflection curves within the web to experimental test values. The experimental radial deflections were measured at $D/4$, $D/2$ and $3D/4$ where D is the depth of the web. These measurements were taken at the mid-length of the web panels. The maximum FEA radial deflections occur approximately at the mid-length of the critical panel and approximately at a depth of $D/2$ in all the girders. The load–radial deflection curves do not indicate when the FEA shear buckling load is exceeded within the full nonlinear solutions.

A diagonal wave pattern forms as the shear force in the panel increases. To illustrate, Fig. 17 gives a deformed shape of girder S2 when location 2L reaches 51 mm (2 in.) vertical deflection.

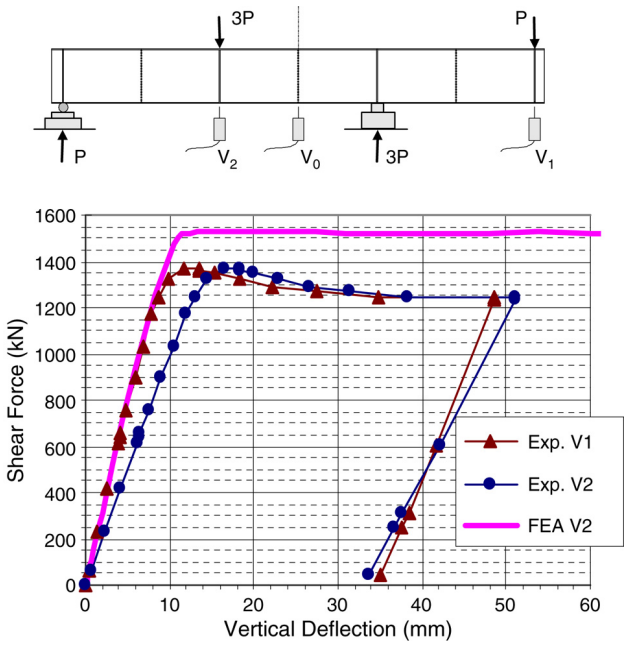

Fig. 10. Girder S1-S — load–vertical deflection curves at the applied-load locations.

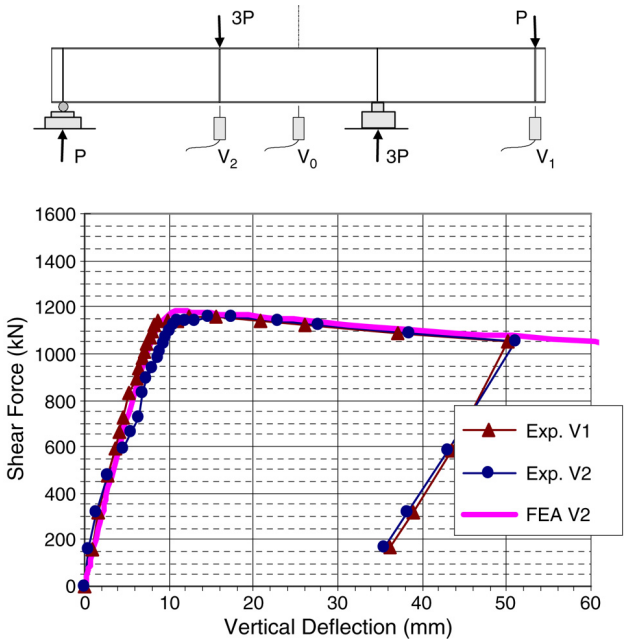

Fig. 11. Girder S2 — load–vertical deflection curves at the applied-load locations.

As can be seen from Fig. 17, the radial displacements of the webs in the FEA models are predominantly toward the center of curvature of the girders. This behavior is the same as that observed within the physical tests, and is initially associated with a straightening out of the web panels along the diagonal tension direction. Due to the compression along the opposite diagonal direction within the web panels, the critical panel eventually exhibits a bulge toward the center of curvature that is larger than that associated with the simple straightening

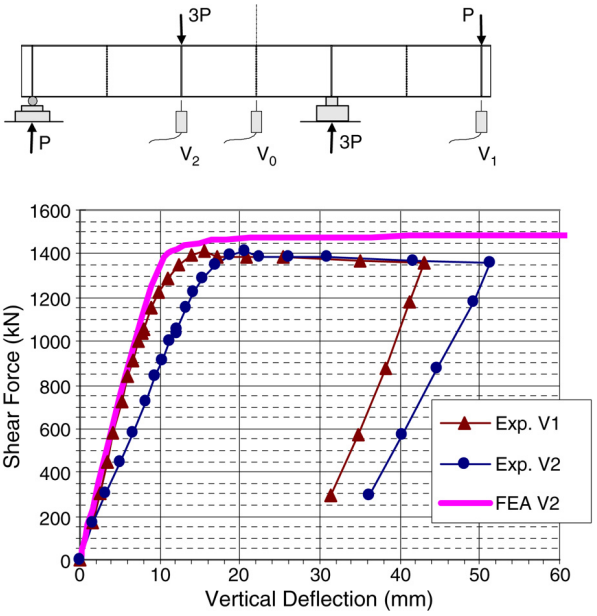

Fig. 12. Girder S2-S — load–vertical deflection curves at the applied-load locations.

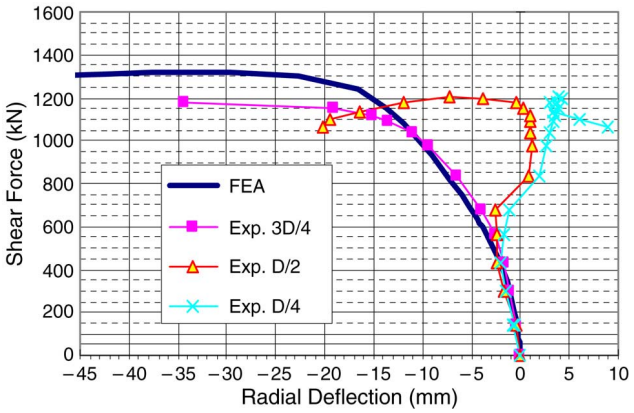

Fig. 13. Girder S1 — radial displacement at the middle of the panel B versus shear force.

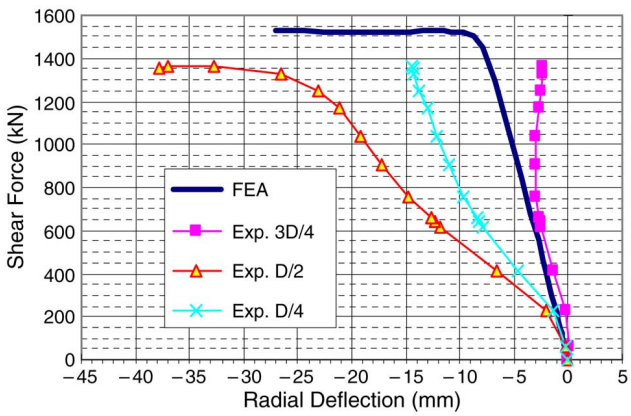

Fig. 14. Girder S1-S — radial displacement at the middle of the critical panel versus shear force.

out of the web panel along the tension diagonal, both in the experiments and in the FEA.

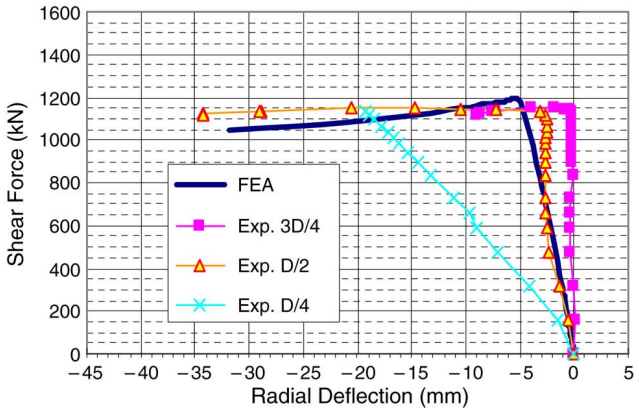

Fig. 15. Girder S2 — radial displacement at the middle of the panel B versus shear force.

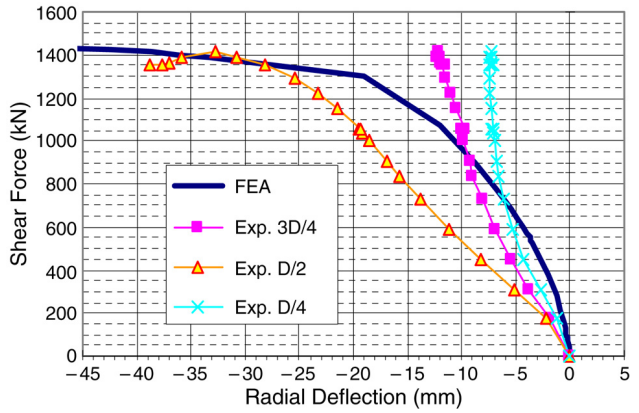

Fig. 16. Girder S2-S — radial displacement at the middle of the critical panel versus shear force.

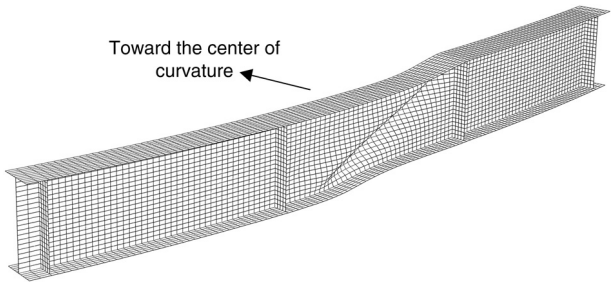

Fig. 17. Deformed shape of girder S2 using the first mode for the specified imperfection when location 2L reaches 51 mm (2 in.) vertical deflection (deformation scale factor = 2.0).

5.2.2. Strains and von Mises stresses in web panels

The strains within the critical web panels exhibit the same general trends in both the FEA and the physical tests. The reader is referred to [15] for comparisons of these detailed responses. However, the correlation between the detailed FEA and experimental local strains within the web panels is generally poor. This is believed to be due to a sensitivity of localized inelastic strains to precise initial conditions. At the peak capacity level of the girders with $d_o/D = 1.5$, the principal membrane tension orientation is approximately the same as the angle between the corners of the web panel in both the FEA and the experimental tests. Conversely, the average membrane tension orientation for the girders with $d_o/D = 3$ is somewhat larger (steeper) than the angle between the corners of the web panel in both the FEA and the experiments. Once the girders are deformed into the post-peak region, the principal strain orientations tend to decrease for all of the girders, both analytically and experimentally.

Equivalent plastic strain contour plots from the analyses show that the onset of yielding through the entire thickness of the web panel occurs along the tension band approximately at the peak capacity level in all the test girders [15]. Within the post-peak range of the response, the width of the yielded diagonal band generally increases as the overall inelastic vertical displacements of the girders increase. In the girders with $d_o/D = 1.5$, the yielded band tends to expand across the transverse stiffener location and into the adjacent less critical web panel.

In all of the girders, the computed and the experimentally measured distortions are relatively minor at the peak load level. These distortions become more significant within the plateau or post-peak range of the response.

6. Parametric studies

In the experimental tests of the four girders, the flange dimensions were selected to ensure that a web shear failure would occur rather than a flange lateral bending failure. An important question that should be asked is whether the maximum shear strength of curved I-girders subjected to high web shear can be adversely affected by flange lateral bending associated with the horizontal curvature. In other words, it should be questioned as to whether the restraint provided to the web panels by the flanges could be lost due to the influence of flange lateral bending to an extent such that the web shear strength is significantly reduced. If the flange sizes are reduced significantly, some decrease in the shear strength is expected within straight I-girders. That is, some interaction between the shear and major-axis bending strengths of straight I-girders is expected. However, these moment–shear interaction effects have been shown to be small enough to be neglected within the context of the AASHTO (2004) shear strength formulas [24–27]. If significant flange lateral bending exists, it is possible that some interaction between the girder vertical bending, flange lateral bending, and web shear strengths may exist. AASHTO [2] provides simple equations for the major-axis bending strength that account for the influence of (or interaction with) flange lateral bending. These equations, which have been termed the one-third rule, are based in large part on the research reported in [24].

Of the potential geometric variables, the flange width is taken as the sole variable for investigating the influence of flange size on the shear strength behavior of the curved I-girders. The flange widths are reduced from the values employed in the physical tests by Zureick et al. [28] down to the smallest flange width allowed by AASHTO [2], i.e., $D/6 = 203.2$ mm (8 in.) based on the nominal depth of the test girder webs. Strengths for flange widths of 355.6 mm (14 in.), 304.8 mm (12 in.), and 254 mm (10 in.) are reported.

Other flange widths between 355.6 mm and the widths used in the experimental tests have been analyzed, but the strengths for these widths are not reported because the changes in the controlling shear strengths from those associated with the physical tests are small. Also, the widths of the bearing and intermediate stiffeners are adjusted based on the reduced flange width such that the ratio of the flange and stiffener widths is constant. Specifically, the ratio of the flange and the bearing stiffener widths is fixed at 1/0.4 and the ratio of the flange and intermediate stiffener widths is fixed at 1/0.3. These specific ratios are selected to simplify the FEA modeling, but also they result in values for the stiffener areas that violate the [2] area requirements for transverse stiffeners in some of the cases considered with smaller flanges. In all cases, the [2] transverse stiffener rigidity and bearing stiffener provisions are satisfied.

In the AASHTO [2] strength calculations, the interior segment of the girders between locations 2L and 2R is critical with respect to shear, since equal panel d_o/D values are used throughout the girders and the web shear within the interior segment is twice that within the outside unsupported lengths (see Fig. 1). However, with respect to the calculation of the major-axis bending strength M_n per AASHTO [2], the outside segments are more critical with respect to lateral–torsional buckling (LTB). Based on a C_b value of 1.75 for the exterior segments (versus 2.3 for the interior one), the effective length factor for the exterior segments based on LTB buckling strength of the three-segment specimens as a whole is estimated using the procedure proposed by Nethercot and Trahair [21] and Galambos [29] as $K = 0.919$. However, based on either $K = 0.919$ or conservatively $K = 1$ for the exterior segments along with $C_b = 1.75$, the AASHTO [2] LTB strength never governs for any of the girders considered in this study (unbraced lengths large enough such that the flexural resistance would be reduced due to LTB would generally preclude the development of a shear failure). The strength of girders in the parametric study is governed either by shear or by flange local buckling or yielding in flexure.

When the geometric proportions of the test girders are used, the flexural strengths are reduced slightly due to flange local buckling. However, for all the other cases, the girder flexural strengths per AASHTO [2] in terms of the major-axis bending moment are simply

$$M_{n(1/3\text{ rule})} = (R_b F_{yc} - f_\ell/3) S_{xc} \tag{3}$$

where R_b is the strength reduction factor that accounts for web post-bend buckling and load shedding effects, F_{yc} is the compression flange yield strength, f_ℓ is the elastically computed flange lateral bending stress at the maximum load level from the full nonlinear FEA solutions, and S_{xc} is the elastic section modulus to the compression flange. The Engineer should note that the above definition of $M_{n(1/3\text{ rule})}$ is equivalent to but is written in a slightly different format than that in [2]. The influence of the flange lateral bending is included on the right-hand side of Eq. (3) in the calculation of the major-axis bending resistance. In [2], the applied flange lateral bending stress (or moment) is included with the vertical bending stress (or moment) on the left-hand side of the LRFD

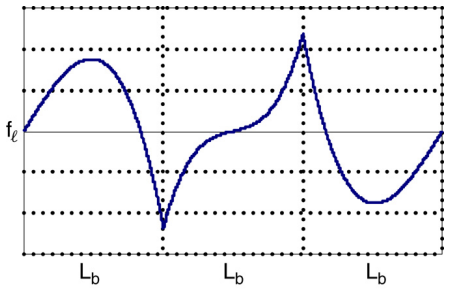

Fig. 18. Typical flange lateral bending stress variation along the girder length based on open-walled section beam theory.

strength equation. The flange yield strength F_{yc} is used in the calculation of the girder R_b values in Eq. (3) as recommended in [2]. The commentary of [2] allows the Engineer to obtain a more refined value of R_b by substituting the strength of the compression flange, F_n, based on $R_b = 1$ for the flange yield strength. This more refined procedure gives a larger R_b value for the experimental girder dimensions, where the flanges are noncompact; however, in all the other cases, F_n based on $R_b = 1$ is equal to F_{yc}. Nevertheless, the smallest R_b value for all of the girders (even for $b_f = 203.2$ mm (8 in.)) is only 0.978.

The flange elastic lateral bending stress f_ℓ in Eq. (3) is calculated from a first-order elastic analysis using open-walled section beam theory and is then amplified by a corresponding simple amplification factor equation provided in [2] to account for second-order effects. As discussed in [2], this amplification factor is typically a conservative estimate of the true second-order elastic amplification of the flange lateral bending stresses in cases where these effects become significant. With the exception of the girders with $b_f = 203.2$ mm (8 in.) and 254 mm (10 in.), the AASHTO [2] amplification factor (AF) is equal to 1.0 in this study. To illustrate the effect of AF, the strengths $M_{n(1/3\text{ rule})}$ based on both AF > 1.0 and AF $= 1$ are included in the reported results for the girders with the above b_f values.

A representative plot of the flange lateral bending stresses for the test configuration considered in this work is shown in Fig. 18. The flange lateral bending stress may be calculated in general from open-walled section beam theory as

$$f_\ell = \frac{B\omega}{C_w} \cong \frac{M_\ell h \left(\frac{h}{2}\frac{b_f}{2}\right)}{\left(\frac{I_{yc}h^2}{2}\right)} = \frac{M_\ell \frac{b_f}{2}}{I_{yc}} \tag{4}$$

where B is the section bimoment, ω is the principal sectorial coordinate at the flange tips, C_w is the warping constant of the cross-section, M_ℓ is the corresponding flange lateral bending moment, h is the distance between the mid-thickness of the flanges, b_f is the flange width, and I_{yc} is the moment of inertia of the individual flanges about a vertical axis through the web.

White et al. [24] observe that if the I-girder flexural strength is quantified by the one-third rule, no further interaction between the major-axis bending strength and web shear needs to be considered for cases in which the web is subjected to high shear forces. This portion of the paper seeks to test these observations within the context of variations on the geometry

of the curved I-girder experiments conducted by Zureick et al. [28].

Other various FEA parametric studies are conducted. First, the test girders are analyzed with and without the residual stresses included in the models to ascertain the influence of representative residual stresses on the shear strength behavior. Second, the influence of the magnitude of the geometric imperfections on the maximum strength behavior of girders S2 and S2-S is investigated. Next, two equivalent straight girders, one corresponding to a girder with $d_o/D = 3$ (S2) and the other corresponding to a girder with $d_o/D = 1.5$ (S2-S), are considered, with the intent to examine the shear behavior in the limit that the radius of curvature becomes infinite. The overall dimensions and material properties used to generate the straight girder models are the same as those of the curved I-girders S2 and S2-S except that the horizontal radius of curvature is set to infinity. This provides additional data for evaluation of the effects of horizontal curvature. These equivalent straight girders are studied with several different geometric imperfections to ascertain the sensitivity of the response to these imperfections.

The results from the above parametric analysis studies are summarized below.

6.1. Effects of reduced flange and stiffener sizes on elastic buckling strengths

When the flange widths are reduced from the original test dimensions to the smallest values allowed by AASHTO [2] (i.e., $b_f = D/6 = 203.2$ mm (8 in.)), the elastic buckling strengths are generally decreased. The smallest reduction is 9.26% for one of the girders with $d_o/D = 3$, and the largest reduction is 13.33% for one of the girders with $d_o/D = 1.5$. In spite of these strength reductions, the AASHTO [2] provisions are still significantly conservative in predicting the elastic shear buckling strengths for all of the parametric study girders. For example, the buckling capacity based on the AASHTO [2] provisions is only half the FEA buckling solution for S2 with a reduced flange width of 203.2 mm (8 in.). This kind of conservatism can be alleviated and the scatter in the design predictions relative to the refined FEA solutions reduced by the use of the shear buckling coefficient formulae suggested by Lee et al. [16] ([15]).

6.2. Effects of reduced flange and stiffener sizes on maximum strengths for curved I-girders

Figs. 19 through 22 present the girder strengths in the context of a moment–shear interaction plot for each of the girders considered. Two data points are shown for the cases in which the AASHTO [2] amplification factor on the flange lateral bending stresses (AF) is greater than one. The points denoted by the solid diamonds show the $(M_{\max}/M_{n(1/3\text{ rule})}, V_{\max}/V_{n(\text{AASHTO 2004})})$ values based on AF = 1, whereas the open diamond symbols show the values of the $(M_{\max}/M_{n(1/3\text{ rule})}, V_{\max}/V_{n(\text{AASHTO 2004})})$ when AF > 1 and the first-order stresses f_ℓ are amplified by this factor.

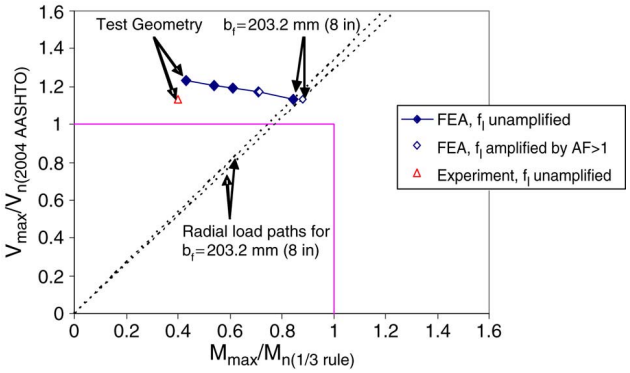

Fig. 19. Girder S1 with variable flange width — moment–shear interaction.

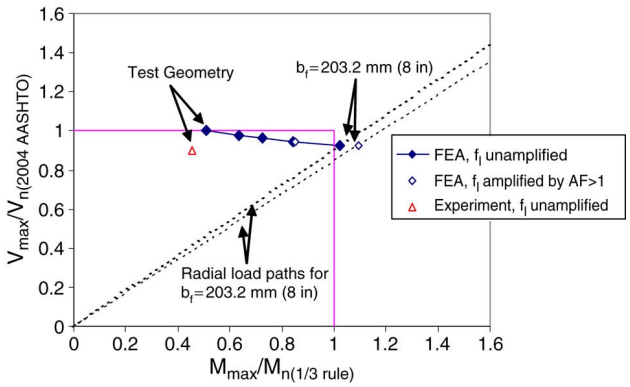

Fig. 20. Girder S1-S with variable flange width — moment–shear interaction.

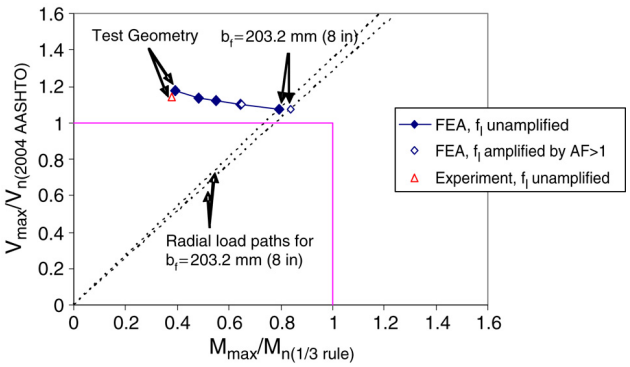

Fig. 21. Girder S2 with variable flange width — moment–shear interaction.

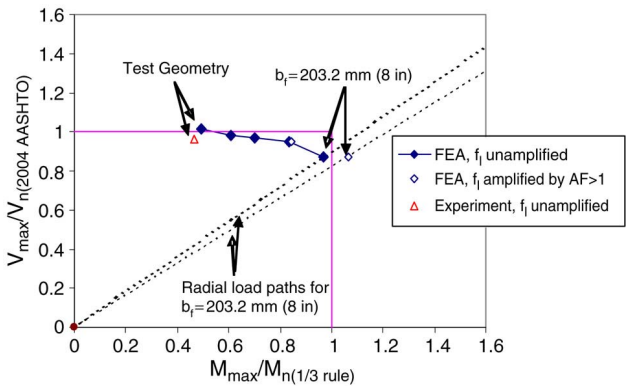

Fig. 22. Girder S2-S with variable flange width — moment–shear interaction.

Also, for the geometry associated with the experimental tests, a data point is included that corresponds to the maximum shear and moment measured within the experiment normalized by the AASHTO [2] V_n and $M_{n(1/3\text{ rule})}$ values, where $M_{n(1/3\text{ rule})}$ is based on Eq. (3) except that F_{yc} is replaced by the base flange local buckling strength (only slightly less than F_{yc}). This point is denoted by the open triangle symbol within the plots.

As the flange width is reduced, it can be seen from Figs. 19–22 that the normalized peak shear capacities are slightly decreased. The use of the smallest flange width allowed by AASHTO [2] ($b_f = D/6 = 203.2$ mm (8 in.)) causes a maximum reduction of 8% for girders S1 and S1-S, 9% for S2 and 14% for S2-S relative to the FEA strengths using the dimensions from [28]. It should be noted that since the flange size does not have any influence on the web panel shear strength per the AASHTO [2] equations, the design shear capacity of a girder is the same for all the different flange widths. Therefore, the variation of $V_{\max}/V_n$ is entirely due to the decrease in the maximum shear developed within the middle test length due to the reduction in the flange size. In contrast, $M_{\max}/M_{n(1/3\text{ rule})}$ varies with decreases in the flange size due to the reduced $M_{\max} = V_{\max}/2L_b$ as well as due to reductions in $M_{n(1/3\text{ rule})}$ associated with (1) the larger calculated elastic flange lateral bending stresses f_ℓ in Eq. (3) caused by the smaller flange widths as well as (2) the reduction in the elastic section modulus to the compression flange S_{xc} due to the smaller flange sizes.

It should be noted that $V_{\max}/V_n$ is larger than $M_{\max}/M_{n(1/3\text{ rule})}$ for most of the girders. When $V_{\max}$ is reduced, $M_{\max} = V_{\max}/2L_b$ is of course also decreased, but this reduction is relatively small. In contrast to the calculation of the AASHTO [2] design shear strength V_n, the design flexural strength $M_{n(1/3\text{ rule})}$ per Eq. (3) is significantly affected by the reductions in the flange size. Therefore, the ratio $M_{\max}/M_{n(1/3\text{ rule})}$ is significantly larger for smaller flange widths. The predominant factor influencing the changes in $M_{\max}/M_{n(1/3\text{ rule})}$ is actually the reduction in the elastic section modulus S_{xc}, not the increase in the flange lateral bending stress. The reduction of the flange width from that of the test girders to the smallest value allowed by AASHTO [2] ($b_f = D/6 = 203.2$ mm (8 in.)) results in a maximum reduction in $M_{\max} = V_{\max}L_b/2$ of 14% (for girder S2-S; see the above discussion regarding the behavior of $V_{\max}/V_n$). However, this reduction in the flange width decreases the elastic section modulus by more than 50% from that of the original test geometry.

The inspection of failure modes within the critical segment shows that the governing failure mode is dominated by web postbuckling shear deformations within the critical web panel except for the girders with the narrowest flange width of 203.2 mm (8 in.). For the girders with flange widths ranging from the test dimensions down to 254 mm (10 in.), all the girders exhibit post-peak deformations that are dominated by web shear postbuckling actions without any substantial flange lateral bending deformations. However, when the flange width is reduced to 203.2 mm (8 in.), the girder deformations are dominated by the web shear postbuckling response up to the peak load level, but significant flange lateral bending deformations occur within the post-peak range of the response. Correspondingly, it can be observed from the moment–shear interaction plots that in the case of girders S1-S and S2-S, the AASHTO [2] governing strength check changes from shear to flexure when b_f is changed from 254 mm (10 in.) to 203.2 mm (8 in.). That is, for $b_f = 203.2$ mm (8 in.), a radial line drawn from the origin through the corresponding data point on the plots intersects $M_{\max}/M_{n(1/3\text{ rule})} = 1$ before it intersects $V_{\max}/V_{n(\text{AASHTO 2004})} = 1$ (see Figs. 20 and 22). These cases correspond to the two data sets of points most to the right side of the plots. For Girders S1 and S2, the AASHTO [2] flexural strength is close to governing for the cases with the smallest flange widths. However, the value of V_n is smaller for these girders due to their wider stiffener spacing, and therefore the shear strength check still controls for these girders with the smallest b_f.

Although there is some decrease in $V_{\max}/V_n$ as the flange widths are reduced in each of the girders as shown in Figs. 19–22, the FEA strengths are predicted quite adequately in all the cases by the AASHTO [2] equations. For girders S1 and S2, the FEA strengths are predicted conservatively by the AASHTO [2] shear strength equations for all the flange widths. For girders S1-S and S2-S, the smallest value of $V_{\max}/V_n$ for the girders that are limited by their shear strength is 0.95 (corresponding to the second set of data points from the right in Figs. 20 and 22 and $b_f = 254$ mm (10 in.)). For these girders and $b_f = 203.2$ mm (8 in.), the strengths are governed by flexure and the smallest value of $M_{\max}/M_{n(1/3\text{ rule})}$ is 0.97 (corresponding to the right-most set of data points in the figures) when AF is taken equal to one. When the AASHTO [2] amplifier is applied to the computed elastic flange lateral bending stresses, $M_{\max}/M_{n(1/3\text{ rule})} = 1.10$ and 1.06 for girders S1-S and S2-S respectively.

The post-peak deformed shapes show clearly that the final FEA failure mode of the girders with $b_f = 203.2$ mm (8 in.) is lateral–torsional buckling (LTB) since the flanges deform in an S-pattern with the compression flange in one of the unbraced segments deflecting toward the center of curvature [15]. Nevertheless, the deformations are dominated by the web shear postbuckling response in all cases at the maximum load level. Therefore, the FEA failure mode for these girders is a combination of shear and flexure failures.

It is noteworthy that, once the flange widths of the girders S1-S and S2-S are reduced to 304.8 mm (12 in.) or less, the intermediate stiffeners start to violate the minimum area requirement specified by AASHTO [2]. Nevertheless, there is no significant reduction in the strength for these girders associated with this violation of the AASHTO requirements. Furthermore, it is interesting to note that the intermediate stiffeners in the deformed geometries of the girders remain stable (i.e., negligibly deformed and holding a “nodal” line in the web) even for the girders with the smallest flange width. It is also of interest to note that the stiffener rigidities based on an assumed 16 mm (5/8 in.) thickness and $0.3b_f$ for the stiffener width are approximately two times the AASHTO [2] rigidity

requirement even for the smallest flange and stiffener widths (i.e., $b_f = 203.2$ mm (8 in.)).

6.3. Effects of reduced flange and stiffener sizes on shear strength and moment–shear interaction for equivalent straight I-girders

Two groups of straight girders corresponding to girder S2 with $d_o/D = 3$ and girder S2-S with $d_o/D = 1.5$ are investigated for the effects of reduced flange size on the strength and behavior of the girders. Figs. 23 and 24 present the data in the context of a moment–shear interaction plot. The girder post-peak deformations are dominated by web shear failure except for the girder with $d_o/D = 1.5$ and $b_f = D/6 = 203.2$ mm (8 in.), the failure mode of which is the closest to being governed by flexure instead of by shear. In fact, if the modified AASTHO shear strength is used, a radial line from the origin of the plot to the right-most data point crosses $M_{\max}/M_n = 1$ prior to crossing $V_{\max}/V_n = 1$ (that is, the strength is governed by flexure instead of by shear). This change in the governing strength equations also occurs in Figs. 19 and 21 if the shear capacity is calculated using the modified AASHTO equations.

For the straight-girder equivalents of both S2 and S2-S, the peak shear capacity, $V_{\max}$, is gradually decreased with the reduction of the flange size. However, similar to the behavior of the curved I-girders, this decrease is rather small. The straight girder equivalents of S2 exhibit the largest reduction, with the decrease in $V_{\max}$ being about 10% from the straight girder with $b_f = 557.3$ mm (21.94 in.) to the one with $b_f = 203.2$ mm (8 in.). The straight girder equivalents of S2-S show a maximum reduction of approximately 7% as the flange width is reduced to the smallest b_f.

Given the same section dimensions, the straight I-girders exhibit somewhat larger shear capacities than the curved I-girders. Consequently, since the same design shear strength is used for either tangent or curved girders, $V_{\max}/V_n$, the ratio of the FEA predictions to the design strengths is generally larger than that for the curved I-girders. These results show that the web panel shear capacities of the I-girders are influenced both by the flange dimensions as well as by horizontal curvature. Nevertheless, the AASHTO [2] equations predict the FEA strengths of all the girders considered in this research either accurately or conservatively.

6.4. Effects of residual stress on maximum strengths

The largest reduction in strength due to residual stresses is only three percent [15]. Also, the effect of the residual stresses is less pronounced in the girders with $d_o/D = 1.5$ compared to those with $d_o/D = 3$. These results are consistent with prior solutions presented by White et al. [24].

6.5. Effects of imperfection magnitude on maximum strengths

Given a specified geometric imperfection pattern, the maximum strengths of the curved I-girders are insensitive to the imperfection magnitude. Also, with the exception of extremely small imperfections, the maximum strengths of the equivalent straight I-girders are not sensitive to the imperfection magnitude. However, when minute imperfections that would be difficult to achieve physically are specified, the FEA solutions of the straight I-girders predict a significant increase in the maximum strength. This behavior is believed to be a manifestation of the inelastic buckling paradox [22,14,6]. Similar results are obtained by Aydemir et al. [25] in the analysis of straight hybrid I-girders. The results reported by Lee and Yoo [17] are also indicative of this phenomenon.

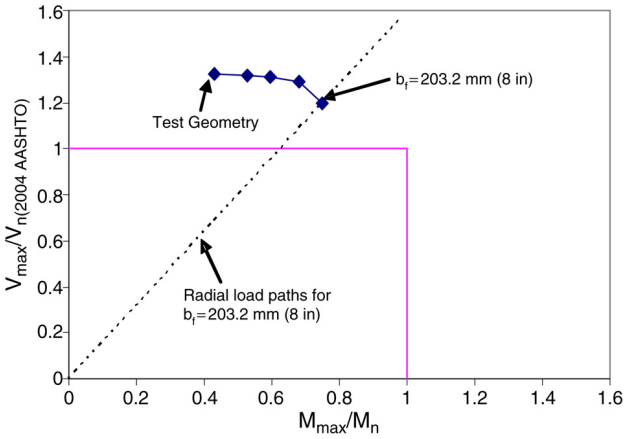

Fig. 23. Equivalent straight girder S2 — moment–shear interaction.

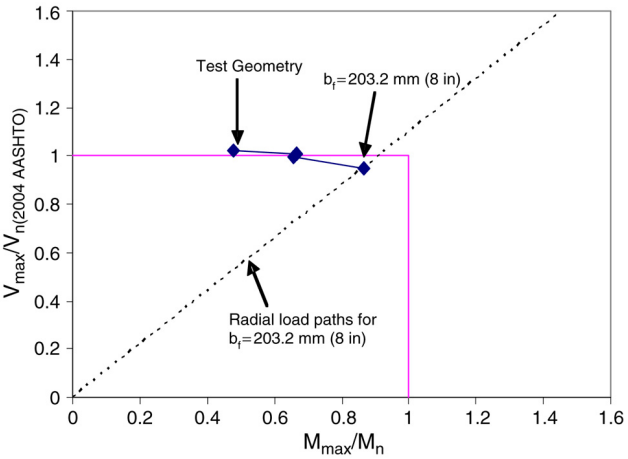

Fig. 24. Equivalent straight girder S2-S — moment–shear interaction.

7. Conclusions

The studies conducted in this paper, combined with the additional FEA studies reported in [24], the experimental test results reported in [28], and the results from other prior research cited in this paper support the following conclusion: transversely stiffened curved I-girders can be designed for maximum strength loading conditions based on the AASHTO [2] I-girder shear capacity equations, including the consideration of postbuckling strength, at least up to the following limits:

- $d_o/D \leq 3$
- $D/t_w \leq 160$
- $d_o/R \leq 0.10$.

Also, the results developed in this research support the conclusions from [24–26], and [27] that moment–shear interaction need not be considered in straight and/or curved I-girders designed using the AASHTO [2] Specifications.

Acknowledgements

The authors express their sincere thanks to Professional Service Industries, Inc. (PSI) and the Federal Highway Administration (FHWA) for their support of this work. Dr. Mohammad S. Khan is the technical contact at PSI and Dr. William Wright is the technical contact at FHWA. Contributions of Professor A.H. Zureick, Dr. N. Phoawanich and Dr. J. Park during the experimental testing phase of this work are acknowledged. The opinions, findings and conclusions expressed in this paper are those of the authors and do not necessarily reflect the views of the above individuals and groups.

References

[1] AASHTO. Guide specifications for horizontally curved steel girder highway bridges with design examples for I-girder and box-girder bridges. Washington (DC): American Association of State and Highway Transportation Officials; 2003.
[2] AASHTO. AASHTO LRFD bridge design specifications. 3rd ed. 2005 Interim Provisions, Washington (DC): American Association of State and Highway Transportation Officials; 2004.
[3] AWS. Structural welding code–steel. AWS D1.1:2000, 17th ed., prepared by AWS Committee on Structural Welding. 2000. 450 pp.
[4] Basler K, Yen BT, Mueller JA, Thurlimann B. Web buckling tests on welded plate girders. WRC Bulletin No. 64. New York (NY): Welding Research Council; 1960. p. 63.
[5] Bradford MA. Improved shear strength of webs designed in accordance with the LRFD specification. Engineering Journal, AISC 1996;33(3): 95–100.
[6] Damkilde L. Elastic-plastic buckling of a finite length cruciform column. Computers & Structures 1985;21(3):521–8.
[7] Davies AW, Griffith DSC. Shear strength of steel plate girders. Proceedings of the Institution of Civil Engineers, Structures and Buildings 1999;134(May):147–57.
[8] Evans HR. Longitudinally and transversely reinforced plate girders. In: Narayanan R, editor. Plated structures — stability and strength. New York (NY): Applied Science Publishers; 1983. p. 1–37.
[9] Evans HR, Porter DM, Rockey KC. The collapse behavior of plate girders subjected to shear and bending. In: IABSE proceedings, P-18/78. 1978. p. 1–20.
[10] HKS. ABAQUS/standard version 6.3-1. Pawtucket (RI): Hibbitt, Karlsson & Sorensen, Inc.; 2003.
[11] Höglund T. Simply supported long thin plate I girders without web stiffeners subjected to distributed transverse load. In: Proceedings of the design of plate and box girders for ultimate strength colloquium. London: IABSE; 1971. p. 85–97.
[12] Höglund T. Strength of steel and aluminum plate girders — shear buckling and overall buckling of plane and trapezoidal webs — comparisons with test. Technical report 1995:4 — steel structures. Stockholm: Department of structural engineering, Royal Institute of Technology; 1995.
[13] Höglund T. Shear buckling resistance of steel and aluminum plate girders. In: Proceedings of the bicentenary conference on thin-walled structures. University of Strathclyde; 1996. p. 1–18.
[14] Hutchinson JW, Budiansky B. Analytical and numerical study of the effects of initial imperfections on the inelastic buckling of a cruciform column. In: Buckling of structures, symposium of the international union of theoretical and applied mechanics. 1976. p. 98–195.
[15] Jung SK, White DW. Shear strength of horizontally curved steel I-girders — finite element studies. Final report to Professional Service Industries, Inc. and Federal Highway Administration, Structural Engineering, mechanics and materials report no. 24c. Atlanta (GA): School of Civil and Environmental Engineering, Georgia Institute of Technology; 2003.
[16] Lee SC, Davidson JS, Yoo CH. Shear buckling coefficients of plate girder web panels. Computers & Structures 1996;59(5):789–95.
[17] Lee SC, Yoo CH. Strength of plate girder web panels under pure shear. Journal of Structural Engineering, ASCE 1998;124(2):184–94.
[18] Lee SC, Yoo CH. Experimental study on ultimate shear strength of web panels. Journal of Structural Engineering, ASCE 1999;125(8):838–46.
[19] Lee SC, Yoo CH. Strength of curved I-girder web panels under pure shear. Journal of Structural Engineering, ASCE 1999;125(8):847–53.
[20] Nakai H, Yoo CH. Analysis and design of curved steel bridges. NY: McGraw-Hill; 1988. p. 673.
[21] Nethercot DA, Trahair NS. Lateral buckling approximations for elastic beams. The Structural Engineer 1976;54(6):197–204.
[22] Onat ET, Drucker DC. Inelastic instability and incremental theories of plasticity. Journal of the Aeronautical Sciences 1952;March:181–6.
[23] Porter DM, Rockey KC, Evans HR. The ultimate load behavior of plate girders loaded in shear. The Structural Engineer 1975;53(8):313–25.
[24] White DW, Zureick AH, Phoawanich N, Jung S-K. Development of unified equations for design of curved and straight steel bridge I girders. Final report to American Iron and Steel Institute Transportation and Infrastructure Committee, Professional Services Industries, Inc., and Federal Highway Administration. Atlanta (GA): School of Civil and Environmental Engineering, Georgia Institute of Technology; October 2001. p. 551.
[25] Aydemir M, White DW, Jung S-K. Shear strength and moment shear interaction in HPS hybrid I-girders. Structural engineering, mechanics and materials report no. 25. Atlanta (GA): School of Civil and Environmental Engineering, Georgia Institute of Technology; April 2004.
[26] White DW, Barker M, Azzizinamini A. Shear strength and moment–shear interaction in transversely-stiffened steel I-girders. Structural engineering, mechanics and materials report no. 27. Atlanta (GA): School of Civil and Environmental Engineering, Georgia Institute of Technology; July 2004.
[27] White DW, Barker M. Shear strength of transversely-stiffened steel I-girders. Structural engineering, mechanics and materials report no. 26. Atlanta (GA): School of Civil and Environmental Engineering, Georgia Institute of Technology; May 2004.
[28] Zureick AH, White DW, Phoawanich N, Park J. Shear strength of horizontally curved steel I girders – experimental tests. Final report to Professional Services Industries, Inc. and Federal Highway Administration; March 2002.
[29] Galambos TV, editor. Guide to stability design criteria for metal structures. 5th ed. New York: Structural Stability Research Council, McGraw-Hill; 1998. p. 910.